

Dynamic modes of morphogen transport

Daniel Aguilar-Hidalgo^{1,2,*}, Zena Hadjivasilou^{1,2}, Maria Romanova-Michaelides², Marcos González-Gaitán^{2,†} and Frank Jülicher^{1‡}

¹*Max Planck Institute for the Physics of Complex Systems*

Nöthnitzer Straße 38, 01187 Dresden, Germany and

²*Department of Biochemistry, Faculty of Sciences,*

University of Geneva, Geneva, Switzerland

Abstract

Morphogens are secreted signaling molecules that mediate tissue patterning and growth of embryonic tissues. They are secreted in a localized region and spread through the tissue to form a graded concentration profile. We present a cell-based model of morphogen spreading that combines secretion in a local source, extracellular diffusion and cellular trafficking. We bring the concept of eigen-modes to the problem of gradient formation to introduce hydrodynamic modes of morphogen transport and characterize the dynamics of transport by dispersion relations of these dynamic eigenmodes. These dispersion relations specify the characteristic relaxation time of a mode as a function of its wavelength. In a simple model we distinguish two distinct dynamic modes characterized by different timescales. We find that the slower mode defines the effective diffusion and degradation as well as the shape of the concentration profile in steady state. Using our approach we discuss mechanisms of morphogen transport in the developing wing imaginal disc of the fruit fly *Drosophila*, distinguishing three transport regimes: transport by extracellular diffusion, transport by transcytosis and a regime where both transport mechanisms are combined.

I. INTRODUCTION

The development of embryonic tissues implicates the collective organization of a large number of cells in space and time. A key question is how such tissues can robustly acquire a particular pattern of morphological structures. Biochemical signals, such as morphogens, play an important role to regulate these morphogenetic phenomena during development [1–3]. Morphogens are secreted in a localized region and spread through the tissue to form graded concentration profiles. A system in which morphogen gradients have been extensively studied is the developing fly wing [4–14]. The developing fly wing is an epithelium, a two-dimensional single layer of cells. The morphogen Decapentaplegic (Dpp) is secreted along a stripe of cells in the center of the wing primordium and exhibits graded concentration profiles at each side of the source [15, 16]. Several mechanisms of transport of Dpp in the tissue have been proposed, including spreading by extracellular diffusion and transcytosis [17, 18].

* Present address: School of Biomedical Engineering, University of British Columbia, Vancouver, British Columbia, Canada V6T 1Z3. Michael Smith Laboratories, University of British Columbia, Vancouver, British Columbia, Canada V6T 1Z4

† marcos.gonzalez@unige.ch

‡ julicher@pks.mpg.de

Transcytosis is defined as a transport regime that involves the internalization of molecules into the cell and their subsequent recycling to the cell surface at a different position.

The dynamics of Dpp in the wing primordium has been studied experimentally using fluorescently labelled Dpp expressed in the normal source region in the developing wing tissue. Fluorescently labelled Dpp (GFP-Dpp) forms a concentration profile that is well described by an exponential with a characteristic decay length that ranges up to 8 cell diameters. The dynamics of Dpp in the tissue can be revealed by fluorescence correlation spectroscopy (FCS) [18] and by fluorescence recovery after photobleaching (FRAP) [17]. In FCS, a laser beam is parked in the interface between cells and the temporal correlations of the fluctuating fluorescence signal are measured to estimate the molecular diffusion coefficient [18]. In FRAP, fluorescence of GFP-Dpp is bleached in a region of interest adjacent to the source of production. The recovery of fluorescence over time provides information about the effective diffusion coefficients and degradation rates.

FRAP recovery curves in wild type and in endocytosis defective thermosensitive mutants of *dynammin* suggested that Dpp transport is mediated by endocytic trafficking consistent with transcytosis [17]. In this case the characteristic length of the Dpp profile depends on the effective diffusion coefficient and degradation rate, which themselves are determined by rates of intracellular trafficking. The effective diffusion coefficient measured by FRAP is fundamentally different to the molecular diffusion coefficient in the extracellular space as measured by FCS [19, 20].

However, the shape of the gradient and the dynamics of the FRAP experiments in wild type can be accounted for by a regime of transport in which extracellular diffusion is dominating and is fast. In this case an extracellular gradient would form quickly and the recovery in the FRAP experiment is dominated by the accumulation of molecules intracellularly [18]. While the analysis of endocytosis mutants does not truly support an extracellular diffusion regime [17], with the available assays we cannot currently distinguish between the two regimes of transport, namely a regime where the gradient shape is dominated by extracellular diffusion alone and a regime where intracellular trafficking contributes significantly to the shape of the gradient.

The difficulty in distinguish between the two regimes stems largely from the fact that the FRAP recovery curves can be interpreted in different ways depending on which theoretical model is considered. This has created controversies and divisions in the field with two

different perspective in the interpretation of FRAP data to identify between transport mechanisms. In one case the FRAP dynamics is interpreted as revealing an effective diffusion and an effective degradation, in the other case the FRAP dynamics corresponds only to the dynamics of accumulation of intracellular molecules that do not return to the extracellular space.

Here, we develop a theoretical framework to capture both extreme regimes of transport as well as combinations of the two. This is achieved by considering at the same time extracellular diffusion, internalization, recycling and degradation in a model based on discrete cells, intracellular/extracellular pools and different rates of trafficking between them. In this approach we introduce the concept of hydrodynamic modes of transport which are eigenmodes of the system that decay with characteristic relaxation times that depend of the wavelength of the mode. From the mode structure of the system we can identify the effective diffusion coefficient and degradation rate that govern the slow dynamics and that are not necessarily the same as the diffusion and degradation measured by FCS or FRAP. Additionally, we find a relation between the slow mode of transport and the shape of the steady-state gradient. Using this approach we find that the extreme transport regimes correspond to different values of the trafficking parameters. This framework will help to design the proper assays to parametrize these rates and to determine which actual transport regime underlies gradient formation.

II. DISCRETE MODEL FOR MORPHOGEN TRANSPORT

We present a general cell-based model for the transport of ligand molecules. The discrete nature of this model allows the analysis of the transport dynamics while preserving intrinsic length-scales of the system such as the cell size, which can be lost in continuum schemes as they represent approximations of the more realistic cell-based model.

A. Dynamic equations of the transport model

We present a general cell-based model for the transport of ligand molecules that are secreted locally and spread along one axis of the tissue, which consists of a row of cells of size a , and specify a morphogen production and secretion of free ligands region of size

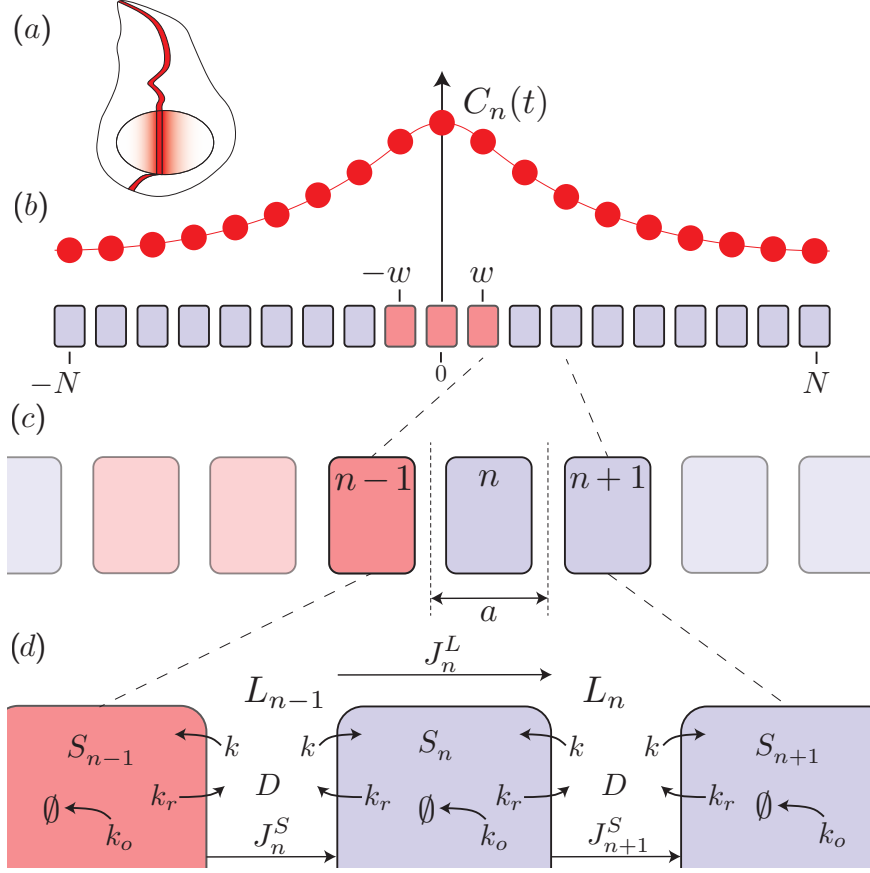


FIG. 1. **Scheme of the morphogen transport model with two compartments.** (a) The wing imaginal disk of the fruit fly is a two-dimensional epithelial sheet with a source releasing Dpp molecules (red) at the anterior-posterior (AP) compartment boundary (dark red), which is approximately linear. As a result of this localized source and Dpp being degraded in the whole tissue, Dpp shows a concentration gradient in the AP direction, which allows its study in one dimension. (b) Discrete profile of morphogen molecules per cell $C_n(t)$, represented by red dots, for an array of $2N + 1$ cells (purple and red boxes), from cell number $n=-N$ to cell number $n=N$. We define a centered morphogen source (red cells) of width $2w + 1$. (c) We define the cell size a as the distance between two subsequent mid-position of the extracellular space. (d) The extracellular pool contains L_n molecules per cell compartment n . These molecules can hop directly from one gap between the cells to the adjacent ones at a rate $2D/a^2$. This describes their free diffusion in the extracellular space around the cells with diffusion coefficient D , which corresponds to non-directed transport (Brownian motion) in the extracellular space in three dimensions which effectively leads to a diffusion coefficient in one dimension. Molecules can be internalized with rate k and recycled back with rate k_r . The intracellular pool of molecules is denoted S_n . Intracellular molecules disappear from the pool at rate k_o . Two transport fluxes J_n^L and J_n^S are defined in eqs. (4) and (5).

$(2w + 1)a$ placed in the center of the tissue, where ligands enter the extracellular space at flux per cell ν . We denote by L_n the number of ligand molecules in the extracellular space between cell n and cell $n + 1$, and by S_n the number of molecules in cell n , see fig. 1. The dynamic equations for these molecule numbers read:

$$\frac{dL_n}{dt} = \frac{D}{a^2} (L_{n+1} - 2L_n + L_{n-1}) + \frac{k_r}{2} (S_n + S_{n+1}) - kL_n + \frac{1}{2} (\nu_n + \nu_{n+1}) \quad (1)$$

$$\frac{dS_n}{dt} = \frac{k}{2} (L_{n-1} + L_n) - k_r S_n - k_o S_n, \quad (2)$$

These equations apply for L_n if $-N - 1 \leq n \leq N$ and for S_n if $-N \leq n \leq N$. Here D is an extracellular diffusion coefficient, k is an internalization rate, k_r is a recycling rate, and k_o is a degradation rate.

We also need to specify the boundary conditions. When solving the equations for L_{-N-1} and L_N we use the boundary values $S_{-N-1} = S_{-N}$, $S_{N+1} = S_N$, together with $L_{-N-2} = L_{-N}$ and $L_{N+1} = L_{N-1}$, which corresponds to no flux at the boundaries.

The total number of morphogen molecules per cell is

$$C_n = \frac{1}{2} (L_{n-1} + L_n) + S_n. \quad (3)$$

We will study the system in a finite field of $2N + 1$ cells centered around the source of width $(2w + 1)a$, which contains $2w + 1$ source cells, see fig. 1. Thus our system constitutes a set of $2(2N + 1)$ linear differential equations.

B. Ligand balance due to production, transport and degradation

We now discuss the balance of ligand molecules due to transport, sources and sinks. The currents of extracellular and intracellular ligands are defined as

$$J_n^L = -\frac{D}{a^2} (L_n - L_{n-1}) \quad (4)$$

$$J_n^S = -\frac{k_r}{2} (S_n - S_{n-1}). \quad (5)$$

The dynamic eqs. (1) and (2) define the balance of molecule number C_n

$$\frac{dC_n}{dt} = \frac{1}{2} (J_{n-1}^L - J_{n+1}^L) + \frac{1}{2} (J_n^S - J_{n+1}^S) - k_o S_n + \frac{1}{4} (\nu_{n-1} + 2\nu_n + \nu_{n+1}). \quad (6)$$

This equation confirms the definition of currents J_n^L and J_n^S , and we can identify the degradation rate k_o and the effective source term $(\nu_{n-1} + 2\nu_n + \nu_{n+1})/4$ at cell n .

C. Decomposition in hydrodynamic transport modes

We use a Fourier representation for the morphogen profiles with no-flux boundary conditions. The general solution to the dynamic eqs. (1) and (2) can be written as

$$\begin{pmatrix} L_n \\ S_n \end{pmatrix} = \begin{pmatrix} L_n^{ss} \\ S_n^{ss} \end{pmatrix} + \sum_{\alpha=1}^2 \sum_{m=-N}^N a_m^\alpha \begin{pmatrix} L_m^\alpha \\ S_m^\alpha \end{pmatrix} e^{iq_m n} e^{-s_\alpha(q_m)t}. \quad (7)$$

The boundary conditions used are satisfied for the wave numbers

$$q_m = \frac{2\pi m}{2N+1}, \quad (8)$$

where $m = -N \dots N$. In eq. (7), the time-independent terms are the steady-state profiles L_n^{ss} and S_n^{ss} which the system reaches at long times. The time-dependent terms are relaxation modes of wave number q_m and wavelength dependent relaxation rate $s_\alpha(q_m)$, where $\alpha = 1, 2$ is a mode index. The mode amplitudes are denoted a_m^α . They are in general complex numbers that obey $a_{-m}^\alpha = (a_m^\alpha)^*$, where the star denotes the complex conjugate. The relaxation rates s_α and the eigenmodes (L_m^α, S_m^α) follow from an eigenvalue problem:

$$M(iq) \begin{pmatrix} L^\alpha \\ S^\alpha \end{pmatrix} = -s_\alpha \begin{pmatrix} L^\alpha \\ S^\alpha \end{pmatrix}. \quad (9)$$

Here $M(z)$ with $z = iq$ is the matrix

$$M = \begin{pmatrix} -k + \frac{D}{a^2}(e^{-z} - 2 + e^z) & k_r(1 + e^z)/2 \\ k(1 + e^{-z})/2 & -k_r - k_o \end{pmatrix}, \quad (10)$$

the relaxation rates s_α are the eigenvalues of M , and (L^α, S^α) are the eigenvectors. The eigenvalue problem (9) is solved using $\det(M - \mathbb{I}s) = 0$, where \mathbb{I} is the identity matrix. This equation defines a polynomial in s , which is the characteristic polynomial of the eigenvalue problem

$$s^2 - (k + k_r + k_o)s + kk_o - 2 \left(\frac{kk_r}{4} + \frac{D}{a^2}(k_r + k_o - s) \right) (\cosh z - 1) = 0, \quad (11)$$

Equation (11) has two solutions for two different values s_α of s per wavenumber $z = iq$, which are two eigenvalues s_α that define two different relaxation times in the transport dynamics at different length-scales. The corresponding eigenvectors (L^α, S^α) can then be determined from (9). The full set of modes (L_m^α, S_m^α) with eigenvalues $s_\alpha(q_m)$ then follows by using $q = q_m$ for all $-N \leq m \leq N$.

D. Steady state concentration profiles

At long time, the dynamics of the system reaches a time-independent steady state. The steady-state morphogen profiles provide the shape of the distribution of molecules in the long-time limit.

For a source with constant production $\nu_n = \nu$ for $-w \leq n \leq w$ and $\nu_n = 0$ outside the source region, the steady-state solution can be expressed in regions of constant ν in the form

$$\begin{pmatrix} L_n^{ss} \\ S_n^{ss} \end{pmatrix} = \begin{pmatrix} L^0 \\ S^0 \end{pmatrix} + \begin{pmatrix} L^- \\ S^- \end{pmatrix} e^{-n\sigma} + \begin{pmatrix} L^+ \\ S^+ \end{pmatrix} e^{n\sigma}, \quad (12)$$

with constant (L^0, S^0) in the source region, and where (L^\pm, S^\pm) are the amplitude of the positive and negative exponential contributions to the spatial concentration profile, respectively.

We can use this solution to construct the full concentration profile in a piecewise manner. We need to match together the three regions for $-N \leq n \leq -w$ at the left side of the source, $-w \leq n \leq w$ at the source and $w \leq n \leq N$ at the right side of the source such that they obey the dynamic equations at the source boundaries. Additionally, boundary conditions apply as stated above.

The decay rate σ is determined from the condition $\det(M(z = \sigma)) = 0$, which holds for steady states. We then find

$$\cosh \sigma = \frac{1}{2} \left[\frac{k_r}{4k_o} + \frac{D}{ka^2} \left(1 + \frac{k_r}{k_o} \right) \right]^{-1} + 1. \quad (13)$$

We can define the decay length of the graded distribution of molecules outside of the source

$$\lambda = \frac{a}{\sigma}. \quad (14)$$

If λ is larger than the cell size a , the decay length can be approximated as

$$\lambda \approx \left[\frac{a^2 k_r}{4 k_o} + \frac{D}{k} \left(1 + \frac{k_r}{k_o} \right) \right]^{1/2}. \quad (15)$$

We find that the decay length λ contains two terms. The first corresponds to the contribution of recycling at rate k_r to the formation of the gradient in the absence of diffusion. The second term describes the effects of extracellular diffusion D and cellular capture with rate k of morphogen molecules by endocytosis; it also includes effects of recycling, which makes intracellular molecules available again to diffuse extracellularly. We will analyze this further in the next section. See Appendix A for details.

E. Relaxation time spectrum of the transport equations

The general solution of the transport equation eq. (7) expresses the dynamics of the extracellular and intracellular pools of molecules as a superposition of relaxation modes. The corresponding relaxation rates are given by $s_\alpha(q_m)$, for each wavenumber $q = q_m$. These relaxation rates read

$$s_{1,2} = \frac{1}{2}(k + k_r + k_o) + \frac{D}{a^2}(1 - \cos q) \pm \left[\left(\frac{1}{2}(k + k_r + k_o) - \frac{D}{a^2}(1 - \cos q) \right)^2 - k k_o - 2(1 - \cos q) \left(\frac{k k_r}{4} + \frac{D}{a^2}(k_r + k_o) \right) \right]^{1/2} \quad (16)$$

The functions $s_\alpha = s_\alpha(q)$ defined above are the so-called dispersion relations of the propagating system. An example of the dispersion relations of the two modes $s_{1,2}$ is shown in Figure 2 as a function of q . The mode s_1 is faster than s_2 at all wave-lengths.

F. Effective diffusion constant and effective degradation rate

The dispersion relations introduced in the previous section carry information about how morphogen profiles evolve in time. Of particular interest is the dynamics at long wave-lengths (small wavenumber q), which provides information about the large scale dynamics of the system. To this end, we expand the dispersion relations $s_\alpha(q)$ as Taylor series in the wavenumber q as

$$s_\alpha = K_\alpha + \frac{D_\alpha}{a^2} q^2 + O(q^4) \quad (17)$$

where K_α is the effective degradation rate and D_α is the effective diffusion coefficient in each dynamic mode. The expansions eq. (17) only contain even powers because the transport equations eqs. (1) and (2) do not contain drift terms. As a consequence, q appears in the characteristic polynomial eq. (11) in even functions. We assign $\alpha = 1$ to the faster mode and $\alpha = 2$ to the slower mode. In fig. 3, the curvature of $s_\alpha(q)$ for small q corresponds to the effective diffusion coefficient which can be calculated from eq. (17) as the coefficient of the q^2 -term. We find that the transport model defined in eqs. (1) and (2) in general exhibits two diffusive modes via which molecules can be transported with effective diffusion coefficients D_α and effective degradation rates K_α .

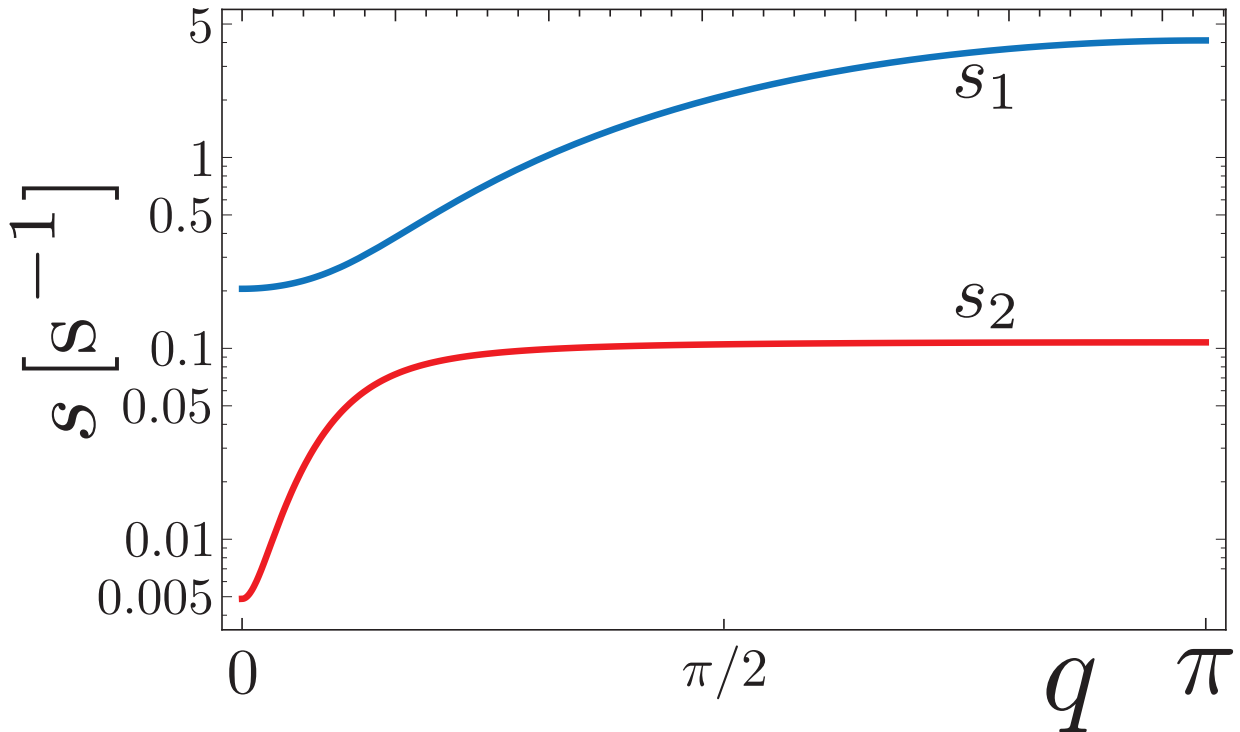


FIG. 2. **Example of dispersion relations.** Shown are the relaxation rate s_1 (blue) of the fast and s_2 (red) of the slow relaxation mode as a function of wave-number q . Parameter values are $D = 1\mu\text{m}^2/\text{s}$, $k = 0.1/\text{s}$, $k_r = 0.1/\text{s}$, $k_o = 0.01/\text{s}$, $a = 1\mu\text{m}$.

G. Dispersion relations in the complex plane

The dispersion relation not only provides information about the relaxation times for given wave number, but also provides information about the steady state. The steady state corresponds to infinite relaxation time $s = 0$. In order to find $s = 0$ we need to extend wave numbers in the complex plane and write $z = \sigma + iq$. Figure 3 shows the real and imaginary parts of $s_{1,2}$ as a function of complex wave number z . The figure shows that only the slow mode s_2 contains a point for which

$$s_2 = 0, \quad (18)$$

which corresponds to the steady state. This occurs for real $z = \sigma = \pm a/\lambda$, defined by the decay length given in eq. (13). Thus, the shape of the distribution of molecules at steady state is determined by the slow relaxation mode s_2 . And the dynamics of the gradient formation at long times is governed by the effective diffusion coefficient D_2 and the effective

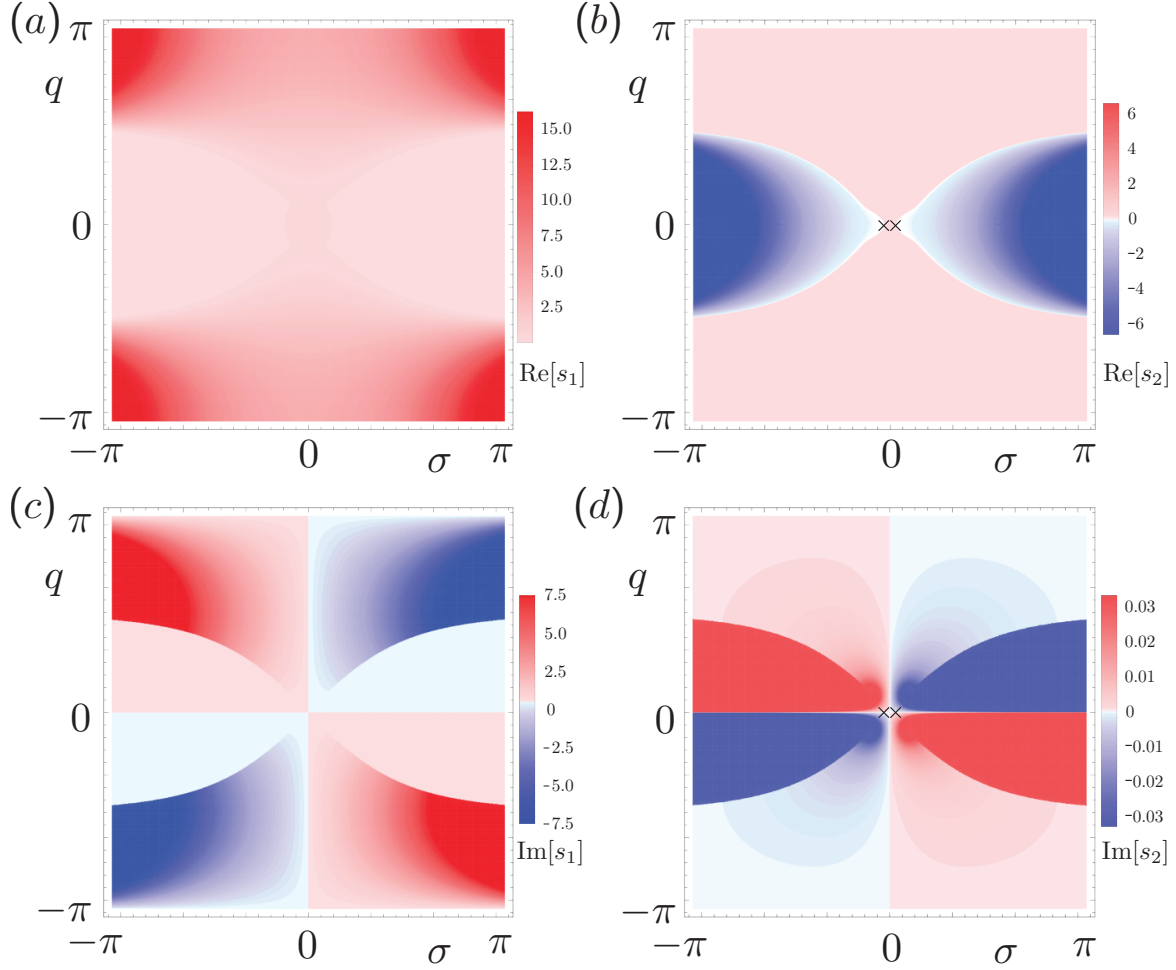


FIG. 3. **Dispersion relations in the complex plane** (a)-(d) Representation in the complex plane of the real ((a) and (b)) and imaginary ((c) and (d)) parts of the complex relaxation rates s_1 ((a) and (c)) and s_2 ((b) and (d)) as a function of complex wave number $z = \sigma + iq$. Values of z for which $s_2 = 0$ are indicated in the real and imaginary parts of s by black crosses. Parameters: $D = 1\mu\text{m}^2/\text{s}$, $k = 0.1/\text{s}$, $k_r = 0.1/\text{s}$, $k_o = 0.01/\text{s}$, $a = 1\mu\text{m}$.

degradation rate K_2 . The steady state is captured approximately when expanding the relaxation rate s_2 for small z as

$$s_2 \approx K_2 - \frac{D_2}{a^2} z^2. \quad (19)$$

The zeros of $s_2 = 0$ correspond to $z = \pm\sigma$ with $\sigma^2 \approx a^2 K_2 / D_2$. This shows that for decay lengths which are large compared to the cell size we have

$$\lambda \approx \sqrt{\frac{D_2}{K_2}}, \quad (20)$$

which corresponds to the decay length for a simple diffusion degradation process.

III. REGIMES OF MORPHOGEN TRANSPORT

The transport model introduced above shows two distinct dynamic modes characterized by different timescales. We now study limit cases of relevance to discuss experiments considered in the literature on morphogens: (i) a scenario of pure transcytosis, in which morphogen transport is driven only via internalization and recycling of molecules in the absence of extracellular diffusion, $D = 0$, and (ii) a scenario of exclusive extracellular diffusion without transcytosis, $k_r = 0$.

A. Pure transcytosis: No extracellular diffusion

In the case without extracellular diffusion, $D = 0$, molecules are transported by internalization and recycling. The dispersion relations are then given by

$$s_{1,2} = \frac{1}{2} \left(k + k_o + k_r \pm \sqrt{(k + k_o + k_r)^2 - 4k(k_o + k_r(1 - \cos q)/2)} \right), \quad (21)$$

The effective degradation rates are

$$K_{1,2} = \frac{1}{2} \left(k + k_o + k_r \pm \sqrt{(k + k_o + k_r)^2 - 4kk_o} \right), \quad (22)$$

and the effective diffusion coefficients are

$$D_{1,2} = \mp \frac{a^2 k k_r / 4}{\sqrt{(k + k_o + k_r)^2 - 4kk_o}}. \quad (23)$$

Here $D_2 > 0$ is the long term effective diffusion coefficient. Note that D_1 is negative. This does not imply an instability in the discrete model presented here. The decay length of the steady-state profile can be approximated as

$$\lambda \approx \frac{a}{2} \sqrt{\frac{k_r}{k_o}}, \quad (24)$$

which depends on the recycling rate k_r and the output rate k_o from the intracellular pool.

B. Pure extracellular diffusion: No recycling of molecules

In the case where no recycling of molecules occurs $k_r = 0$, molecules are transported by extracellular diffusion D only. In this case, the dispersion relations are given by

$$s_1 = k + 2\frac{D}{a^2}(1 - \cos q) \quad (25)$$

$$s_2 = k_o, \quad (26)$$

where the mode s_2 is not diffusive. Thus, transport only occurs via extracellular diffusion via the mode s_1 . From eqs. (25) and (26) we find the effective degradation rates $K_1 = k$ and $K_2 = k_o$, and the effective diffusion coefficients $D_1 = D$ and $D_2 = 0$.

The decay length of the steady-state gradient depends only on the extracellular diffusion coefficient D and on the effective internalization rate k ,

$$\lambda \approx \sqrt{\frac{D}{k}}. \quad (27)$$

Note that contrary to the pure transcytosis case, in the pure extracellular diffusion case λ is independent on the cell size. In this case, molecules internalized to cells do no longer contribute to transport.

C. Extracellular diffusion combined with transcytosis

In this case, both the extracellular diffusion coefficient and the recycling rates are present. This results in a higher complexity of the transport dynamics. The dispersion relations are given by eq. (16). The effective degradation rates are given by

$$K_{1,2} = \frac{1}{2} \left(k + k_o + k_r \pm \sqrt{(k + k_o + k_r)^2 - 4kk_o} \right) \quad (28)$$

and the effective diffusion coefficients read

$$D_{1,2} = \frac{-a^2kk_r/4 + D(k - K_{2,1})}{K_{1,2} - K_{2,1}}. \quad (29)$$

The decay length of the steady-state gradient, as commented in section section IID, contains two independent contributions with dominating recycling rate k_r and extracellular diffusion coefficient D , see eq. (15).

We now discuss these three cases within the context of an application of our theoretical framework in comparison to experiments on the fly wing imaginal disc, see fig. 4.

IV. APPLICATION TO EXPERIMENTAL DATA

Recent literature study the dynamics of fluorescent signals to provide insights on features such as growth control, cellular and molecular patterning, wound repair, and scaling [14, 21–27]. The theoretical framework introduced in the sections above can be applied to such studies to find expressions of time- and length-scales from the analysis of the relaxation time spectrum in rationalized coupled linear systems. This mode structure describes slow and long wavelength modes in the limit of small amplitudes where the underlying nonlinear system can be linearized. In the case of morphogen transport, these time- and length-scales read as the effective degradation rate K_2 , the effective diffusion coefficient D_2 and the decay-length λ of the spatial concentration profile. These quantities are functions of all the parameters of the transport model, and can be inverted to calculate elementary transport rates (D, k, k_r, k_o in our model) from experimentally determine decay-length and effective dynamics. This can be done by tagging the morphogen molecule to a fluorescent molecule and imaging spatial concentration profiles and recording time series of the changes in the fluorescent intensity. Our theory describes average behaviors when averaging over many samples and experiments. It is noteworthy to mention that the transport model can be modified and extended to capture particularities of experimental observations.

A. Application to Dpp in the wing imaginal disc of the fruit fly

As an example of application of the theory presented in previous section, we introduce a particular case of study and further discussion, which requires the addition of extra components in the model, see Appendix B for further example.

1. Dynamics of an immobile fraction

Experimental data of GFP-Dpp concentration profiles and FRAP studies from [17], see figs. 4 and 5 reveal a so-called immobile fraction [17] which relaxes on long time scales. This implies that there is a transfer of molecules from the intracellular mobile pool S_n to an immobile intracellular pool $S_n^{(i)}$ with rate k_i . Then the total rate of molecules $k_o = k_i + k_1$ leaving the mobile intracellular pool S_n is the sum of the immobilization rate k_i and the rate at which molecules are degraded from the mobile intracellular pool k_1 . To study the FRAP

dynamics we update our transport model with a third equation that captures the dynamics of this immobile intracellular pool $S_n^{(i)}$,

$$\frac{dL_n}{dt} = \frac{D}{a^2} (L_{n+1} - 2L_n + L_{n-1}) + \frac{k_r}{2} (S_n + S_{n+1}) - kL_n + \frac{1}{2} (\nu_n + \nu_{n+1}) \quad (30)$$

$$\frac{dS_n}{dt} = \frac{k}{2} (L_{n-1} + L_n) - k_r S_n - k_o S_n, \quad (31)$$

$$\frac{dS_n^{(i)}}{dt} = k_i S_n - k_2 S_n^{(i)} \quad (32)$$

In eq. (32), k_2 denotes the degradation rate in the immobile pool. This immobile pool characterizes a third, non-diffusive, relaxation mode with dispersion relation

$$s_3 = k_2, \quad (33)$$

with effective diffusion coefficient $D_3 = 0$ and effective degradation rate $K_3 = k_2$.

2. Application results and discussion

We can now discuss experimental data on gradients of the morphogen Dpp in the developing wing imaginal disc of the fly. Using a GFP-Dpp construct, the shape of the concentration profiles could be quantified for different stages of development [17]. Quantification of the Dpp profile as a function of the distance of the anterior-posterior compartment boundary is shown in fig. 4a (black dots), together with the profiles calculated for the four different transport scenarios (solid and dashed lines). They correspond to pure extracellular diffusion with small ($D = 0.1\mu\text{m}^2/\text{s}$, solid blue line) and large ($D = 20\mu\text{m}^2/\text{s}$, dashed blue line) diffusion coefficient, pure transcytosis (solid yellow line) and a combination of both (solid red line). Here we consider two different diffusion coefficients in the pure extracellular diffusion scenario to be able to discuss different values suggested in the literature [18], see discussion below. In all cases the decay length is about $\lambda \approx 20\mu\text{m}$.

In order to determine kinetic parameters, fluorescence recovery after photobleaching (FRAP) was performed to quantify the recovery of the bleached fluorescence GFP-Dpp as a function of time. The experimental data are shown in fig. 4b (black dots with error bars) together with calculated FRAP recovery curves for the four transport scenarios discussed above (solid and dashed lines). All four scenarios are consistent with the experimental data shown in fig. 4a and b. Figure 5 shows the FRAP recovery within the first hour.

The calculated recovery curves for the pure transcytosis, the pure extracellular diffusion and the combined transport scenarios are shown as fits to the experimental data, as solid and dashed lines, respectively. The values of the fit parameters as well as the values of the effective diffusion coefficient and effective degradation rate are shown for the four transport scenarios in table I. These parameters are provided as single set estimates per case of study. Uncertainties are large as is reflected in the fact that for the experimental data available, we cannot discriminate between different transport scenarios. The corresponding dispersion relations of transport modes as a function of the wave number q are shown in fig. 5b. They are remarkably different, reflecting the properties of different transport mechanisms and yet they can capture the same dynamics of FRAP recovery and the same steady state profile.

We find that the three transport regimes studied here agree with the full set of experimental data available, namely time-scale for gradient formation close to steady-state [15], the decay-length λ and FRAP recovery curves [17]. The effective diffusion coefficient D_2 and the effective degradation rate K_2 of the slower transport mode obtained for pure transcytosis and combined transport agree with the values estimated in [17]. Future work adding further independent experimental assays will help determine full fits and confidence to the parameters presented here, and will help distinguishing between transport regimes.

V. CONCLUSIONS

We have presented a general cell-based framework for morphogen transport building on an earlier discrete model [8], where we discussed the implication of directional bias in morphogen transport and its effect on explicit ligand-receptor dynamics. Here we bring the concept of eigen-modes to the problem of gradient formation, and studied the mode structure of such a model revealing emergent long wavelength behaviors that cannot be captured by continuum models. Within a common framework, this allows us to study extreme models of morphogen transport that have been debated in the literature. The main controversial point of discussion was whether the shape of the Dpp gradient is solely set by a combination of rapid extracellular diffusion and terminal uptake by cells (pure extracellular diffusion, [28]) or whether uptaken molecules can return to the extracellular space and contribute to the formation of the gradient profile (combined transport [15]). In an extreme limit (pure transcytosis scenario) the molecules do not diffuse extracellularly and are transferred directly

TABLE I. List of parameter values for different transport scenarios considered: Pure transcytosis (yellow), Pure extracellular diffusion with slow (dashed blue) and fast (solid blue) diffusion coefficient, and Combined transport (red). Color references in parenthesis correspond to colors used in fig. 4 and fig. 5a. Parameters are: Extracellular diffusion coefficient D , internalization rate k , recycling rate k_r , output rate k_o of molecules from the intracellular mobile pool, immobilization rate k_i of molecules in the mobile pool, degradation rate k_2 of molecules in the immobile pool, cell size a and the bleaching depth b as the fluorescence intensity at time $t = 0$. Effective diffusion coefficients and effective degradation rates D_2 , K_2 , D_1 , K_1 calculated from eqs. (28) and (29), decay length λ calculated from eq. (15). And R^2 of the fit to the FRAP data ^a

Parameters	Pure transcytosis	Pure extracellular diffusion		Combined transport
D [$\mu\text{m}^2/\text{s}$]	0	0.10	20	20
k [1/s]	0.5	$2.0 \cdot 10^{-4}$	$5.0 \cdot 10^{-2}$	0.5
k_r [1/s]	$6.0 \cdot 10^{-2}$	0	0	$2.4 \cdot 10^{-3}$
k_o [1/s]	$2.5 \cdot 10^{-4}$	$2.5 \cdot 10^{-4}$	$1.5 \cdot 10^{-3}$	$2.5 \cdot 10^{-4}$
k_i [1/s]	$2.5 \cdot 10^{-4}$	$1.25 \cdot 10^{-4}$	$3.0 \cdot 10^{-4}$	$2.5 \cdot 10^{-4}$
k_2 [1/s]	$6.5 \cdot 10^{-5}$	$6.5 \cdot 10^{-5}$	$6.5 \cdot 10^{-5}$	$6.5 \cdot 10^{-5}$
a [μm]	2.6	2.6	2.6	2.6
b	0.14	0.12	0.16	0.16
D_2 [$\mu\text{m}^2/\text{s}$]	0.09	0.10	0	0.10
K_2 [1/s]	$2.2 \cdot 10^{-4}$	$2.0 \cdot 10^{-4}$	$9.0 \cdot 10^{-4}$	$2.5 \cdot 10^{-4}$
D_1 [$\mu\text{m}^2/\text{s}$]	-0.09	0	20	20
K_1 [1/s]	0.56	$2.5 \cdot 10^{-4}$	$5.0 \cdot 10^{-2}$	0.5
D_3 [$\mu\text{m}^2/\text{s}$]	0	0	0	0
K_3 [1/s]	$6.5 \cdot 10^{-5}$	$1.25 \cdot 10^{-4}$	$1.8 \cdot 10^{-5}$	$6.5 \cdot 10^{-5}$
λ [μm]	20.2	22.4	20.0	21.0
R^2	0.98	0.94	0.99	0.99

^a Model parameter values are determine as follows: D is taken from [17] and [18], a is taken from [17], k_2 is estimated from [15] in Pure transcytosis and Combined transport cases. And k is taken from [18] for the case of Pure extracellular diffusion in the scenario of fast diffusion, and b is chosen lower than the first recovery point. Two out of four remaining parameters are estimated from the values of D_2 and K_2 from reference [17], and eqs. (15), (28) and (29). Note that we have given flexibility to these values within their standard deviation interval to heuristically find agreement to the experimental data. This process left two free parameter per case of study.

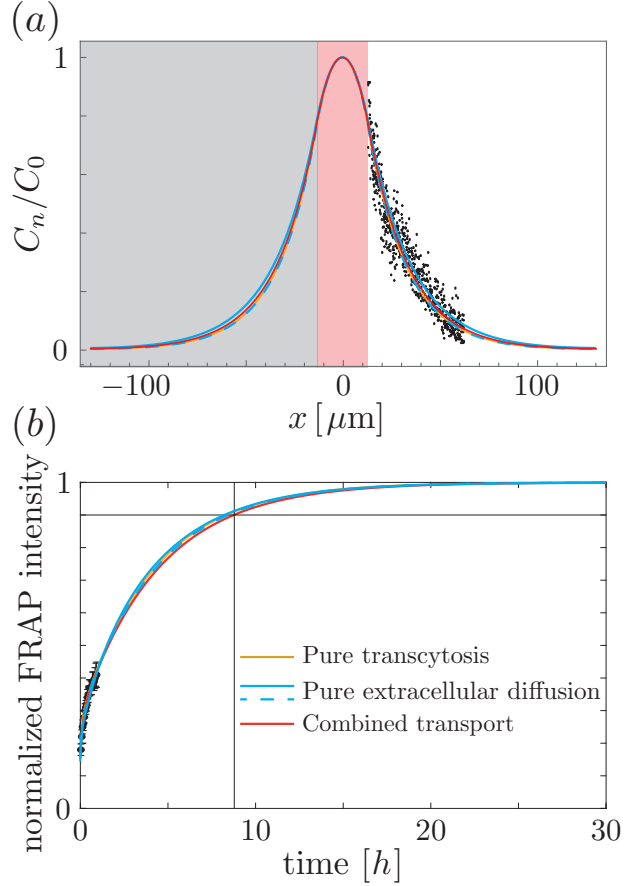


FIG. 4. **Comparison of steady state profiles and FRAP recovery curves between experiment and transport model.** (a) Morphogen profile quantified in [17] (dots) shown together with calculated steady state profiles (solid and dashed lines) for the three transport regimes (color codes for the calculated profiles as in (b)). Red region indicates the source (width $(2w+1)a \approx 10a$). The grey region corresponds to the anterior part of the tissue. (b) Experimentally observed FRAP recovery [17] (dots) shown together with calculated recovery curves for the three transport regimes. Vertical black line indicates $8h$ and horizontal black line, 90% recovery. Experiments showed a 90% recovery after about $8h$ in a pulse chase assay [15]. Parameter values given in table I.

from cell to cell.

Our transport model exhibits two relaxation modes, one fast and one slow, characterized by wave-length dependent dispersion relations. For the slow transport mode we can define an effective diffusion coefficient and an effective degradation rate which govern the large scale dynamics of the concentration profile. These effective transport parameters set the decay length of gradients in steady state and they capture the long time-scale dynamics in

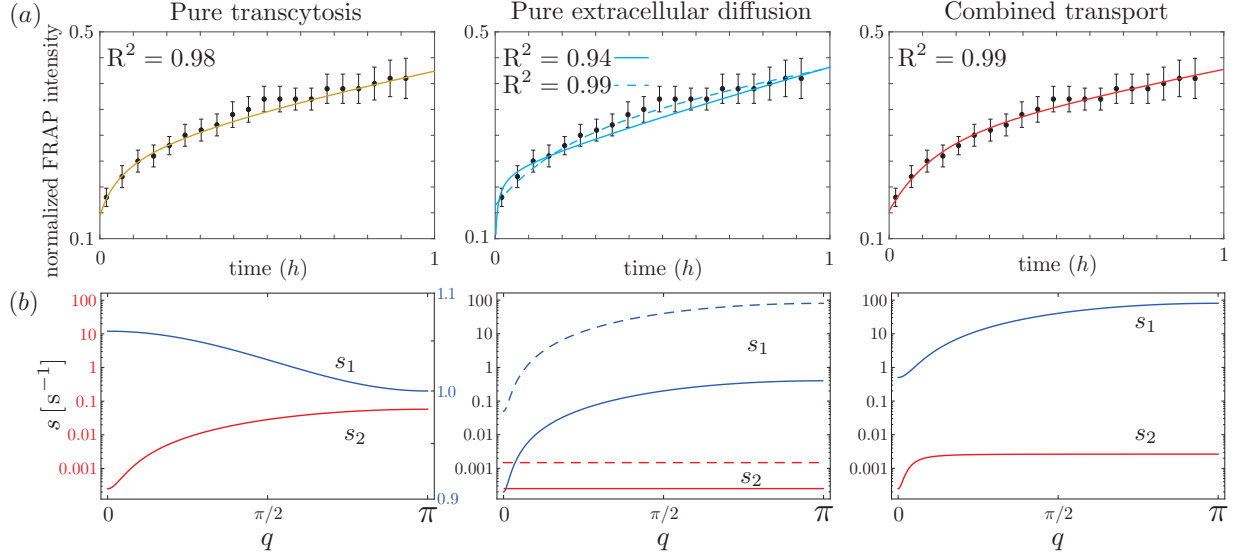


FIG. 5. FRAP recovery curves and corresponding relaxation modes in three transport scenarios. (a) Calculated FRAP recovery curves as a function of time (solid and dashed lines) shown together with experimental data [17] (dots, bars show standard error, 8 samples) for pure transcytosis scenario, pure extracellular diffusion scenario and a combined transport scenario. For the pure extracellular diffusion scenario we show two simulations with slow (solid) and fast (dashed) diffusion coefficient. Parameters indicated in the figure correspond to the scenario with slow diffusion coefficient. The scenario with fast diffusion coefficient corresponds to $D = 20\mu\text{m}^2/\text{s}$ and $k = 5.0 \cdot 10^{-2} \text{s}^{-1}$ [18]. See full parameter sets in table I. (b) Dispersion relations of the relaxation rates as a function of wave-number q corresponding to the calculations shown in (a). Parameter values are given in table I. Parameters are determined to fit the average data with errors.

experiments such as FRAP in the tissue. In contrast, measurements of extracellular diffusion by FCS provide information about one of the parameters in the model, the extracellular diffusion coefficient D . These two parameters (the effective diffusion coefficient D_2 and the extracellular diffusion coefficient D) are conceptually different and can indeed differ significantly in value. For example, in the combined transport scenario $D_2 \simeq 0.1\mu\text{m}^2/\text{s}$ and $D = 20\mu\text{m}^2/\text{s}$, see Fig. 5 and table I. This could account for apparent discrepancies between different types of experiments such as FRAP [17] and FCS [18] that has led to controversies in the field.

This work provides a new framework based on hydrodynamic modes of transport within which to study the dynamics of morphogen gradients and can be used, together with ex-

perimental assays, to bridge gaps and inconsistencies in the field. We discussed how to use different experimental assays (spatial concentration profiles, FRAP, FCS and long time relaxation of morphogen gradient) to estimate values for trafficking parameters. Further transport details can be discussed within the same framework by extending the model, see Appendix B, which will require additional independent experimental assays.

ACKNOWLEDGMENTS

D.A.H. thanks Marko Popovic, Sándalo Roldán-Vargas and Johanna Dickmann for fruitful discussions. D.A.H., F.J. and M.G.G. acknowledge support from the DIP of the Canton of Geneva, SNSF, the SystemsX epiPhysX grant, the ERC (Sara and Morphogen), the NCCR Chemical Biology program and the Polish-Swiss research program. Z.H. was supported by an HFSP Long Term Fellowship. This research was supported in part by the National Science Foundation under Grant No. NSF PHY-1748958, NIH Grant No. R25GM067110, and the Gordon and Betty Moore Foundation Grant No. 2919.01.

Appendix A: Steady state solutions to the transport equations

The steady state solution of eqs. (1) and (2) for a source with constant production rate $\nu_n = \nu$ for $-w \leq n \leq w$ and $\nu_n = 0$ outside the source region, has the form

$$\begin{pmatrix} L_n^{ss} \\ S_n^{ss} \end{pmatrix} = \begin{pmatrix} L^0 \\ S^0 \end{pmatrix} + \begin{pmatrix} L^- \\ S^- \end{pmatrix} e^{-n\sigma} + \begin{pmatrix} L^+ \\ S^+ \end{pmatrix} e^{n\sigma}, \quad (\text{A1})$$

with nonvanishing (L^0, S^0) in the source region. Here (L^\pm, S^\pm) are the amplitude of the positive and negative exponential contributions to the spatial concentration profile, respectively. We distinguish three regions (i) from $n = -N$ to $n = -w$ with amplitudes (L_1, S_1) (ii) from $n = -w$ to $n = w$ with amplitudes (L_2, S_2) and (iii) from $n = w$ to $n = N$ with amplitudes (L_3, S_3) . The amplitudes L_i^0, L_i^-, L_i^+ for $i = 1, 2, 3$ are given by:

$$L_1^0 = 0 \quad (\text{A2})$$

$$L_1^- = L_2^0 \gamma^{-1} (e^{(2w+1)\sigma} - 1) e^{-(w+1)\sigma} (\chi e^\sigma + \tilde{\chi}) \quad (\text{A3})$$

$$L_1^+ = L_2^0 \gamma^{-1} (e^{(2w+1)\sigma} - 1) e^{(2N-w)\sigma} (-\chi - \tilde{\chi} e^\sigma) \quad (\text{A4})$$

$$L_2^0 = L_2^0 \gamma^{-1} \frac{\nu + 2(L_2^- + L_2^+) (-\xi + \tilde{\chi} + \chi \cosh(\sigma))}{-\xi + \chi + \tilde{\chi}} \quad (\text{A5})$$

$$L_2^- = L_2^0 \gamma^{-1} (\chi \cosh((N-w-1)\sigma) + \tilde{\chi} \cosh((N-w)\sigma)) 2e^{N\sigma} \quad (\text{A6})$$

$$L_2^+ = L_2^0 \gamma^{-1} (\chi \cosh((N-w-1)\sigma) + \tilde{\chi} \cosh((N-w)\sigma)) 2e^{(N+1)\sigma} \quad (\text{A7})$$

$$L_3^0 = 0 \quad (\text{A8})$$

$$L_3^- = L_2^0 \gamma^{-1} (e^{(2w+1)\sigma} - 1) e^{(2N-w-1)\sigma} (-\chi - \tilde{\chi} e^\sigma) \quad (\text{A9})$$

$$L_3^+ = L_2^0 \gamma^{-1} (e^{(2w+1)\sigma} - 1) e^{-w\sigma} (\chi e^\sigma + \tilde{\chi}) \quad (\text{A10})$$

with $\gamma = -2(\chi(\exp(2N\sigma) + \exp(\sigma)) + \tilde{\chi}(1 + \exp((2N+1)\sigma)))$, $\chi = D/a^2 + kk_r/(4(k_r + k_o))$, $\tilde{\chi} = -D/a^2 + kk_r/(4(k_r + k_o)) - k/2$, $\xi = k/2$ and decay rate σ as in eq. (13).

The amplitudes of the steady state solution for the intracellular pool are proportional to the amplitudes of the extracellular pool. From eq. (2), we have

$$S_n = \frac{1}{2} \frac{k}{k_r + k_o} (L_{n-1} + L_n). \quad (\text{A11})$$

The amplitudes S_i^0, S_i^-, S_i^+ for $i = 1, 2, 3$ read:

$$S_i^0 = \Omega L_i^0 \quad (\text{A12})$$

$$S_i^- = \Omega L_i^- \quad (\text{A13})$$

$$S_i^+ = \Omega L_i^+. \quad (\text{A14})$$

with $\Omega = k(e^{-\sigma} + 1)/(2k_r + 2k_o)$.

Appendix B: Five-compartment model of morphogen transport

In our approach, it is straightforward to consider additional phenomena in the transport process. Here, we define five pools of molecules, see fig. 6 and eqs. (B1) to (B5). We denote by \bar{L}_n the number of extracellular ligand molecules located between cell n and $n+1$ and not bound to receptors. The number of ligand molecules bound to receptors at the plasma

membrane at the right and left sides of cell n are denoted $S_n^{(r)}$ and $S_n^{(\ell)}$, respectively. The number of ligand molecules internalized upon receptor binding is denoted $S_n^{(e)}$. Molecules in this pool could be degraded, recycled back to the plasma membrane or transferred to a pool of intracellular molecules whose number is denoted $S_n^{(i)}$. The $S_n^{(i)}$ pool can be degraded but does not return to the $S_n^{(e)}$ pool.

1. Dynamic equations

The dynamic equations of the five compartment model read:

$$\frac{d\bar{L}_n}{dt} = \frac{D_0}{a^2} (\bar{L}_{n-1} - 2\bar{L}_n + \bar{L}_{n+1}) + k_{off} (S_n^{(r)} + S_{n+1}^{(\ell)}) - k_{on}\bar{L}_n + \frac{1}{2}(\nu_n + \nu_{n+1}) \quad (\text{B1})$$

$$\frac{dS_n^{(r)}}{dt} = -(k_{off} + \bar{k})S_n^{(r)} + \frac{k_{on}}{2}\bar{L}_n + \frac{k_r}{2}S_n^{(e)} \quad (\text{B2})$$

$$\frac{dS_n^{(\ell)}}{dt} = -(k_{off} + \bar{k})S_n^{(\ell)} + \frac{k_{on}}{2}\bar{L}_{n-1} + \frac{k_r}{2}S_n^{(e)} \quad (\text{B3})$$

$$\frac{dS_n^{(e)}}{dt} = \bar{k} (S_n^{(\ell)} + S_n^{(r)}) - k_r S_n^{(e)} - (k_1 + k_i)S_n^{(e)} \quad (\text{B4})$$

$$\frac{dS_n^{(i)}}{dt} = k_i S_n^{(e)} - k_2 S_n^{(i)}. \quad (\text{B5})$$

These apply for \bar{L}_n if $-N - 1 \leq n \leq N$ and for $S_n^{(r,\ell,e,i)}$ if $-N \leq n \leq N$. Morphogen molecules are produced and secreted to contribute to the \bar{L} pool in the extracellular space with rate ν_n . Molecules of the \bar{L}_n pool diffuse with diffusion coefficient D_0 . They can bind to receptors on the plasma membrane at the left and right side of cells with binding rate k_{on} . Bound ligand can unbind with rate k_{off} and can be internalized with rate \bar{k} into the pool $S_n^{(e)}$. Molecules of the pool $S_n^{(e)}$ can recycle back with rate k_r to the plasma membrane, they can be degraded with degradation rate k_1 or they can be transferred with rate k_i to the immobile pool $S_n^{(i)}$. Finally, the immobile pool is degraded at rate k_2 . For simplicity we choose the boundary conditions as $S_{-N-1}^{(r,e,i)} = S_{-N}^{(\ell,e,i)}$, $S_N^{(r,e,i)} = S_{N+1}^{(\ell,e,i)}$ and $\bar{L}_{-N-2} = \bar{L}_{-N}$ and $\bar{L}_{N+1} = \bar{L}_{N-1}$.

We define the total number of morphogen molecules per cell

$$C_n = \frac{1}{2} (\bar{L}_{n-1} + \bar{L}_n) + S_n^{(r)} + S_n^{(\ell)} + S_n^{(e)} + S_n^{(i)}. \quad (\text{B6})$$

and the currents J_n^L , J_n^S . The current of ligands J_n^L describes the transport of ligand across cells via extracellular diffusion with coefficient D . The current J_n^S describes transport be-

tween cells via binding and unbinding of molecules from receptors on the plasma membrane. These currents read

$$J_n^L = -\frac{D_0}{a^2} (\bar{L}_n - \bar{L}_{n-1}) \quad (\text{B7})$$

$$J_n^S = -k_{off} (S_n^{(\ell)} - S_{n-1}^{(r)}) . \quad (\text{B8})$$

The balance equation for total molecule number then reads

$$\frac{dC_n}{dt} = \frac{1}{2}(J_{n-1}^L - J_{n+1}^L) + \frac{1}{2}(J_n^S - J_{n+1}^S) - k_1 S_n^{(e)} - k_2 S_n^{(i)} + \frac{1}{4}(\nu_{n-1} + 2\nu_n + \nu_{n+1}) . \quad (\text{B9})$$

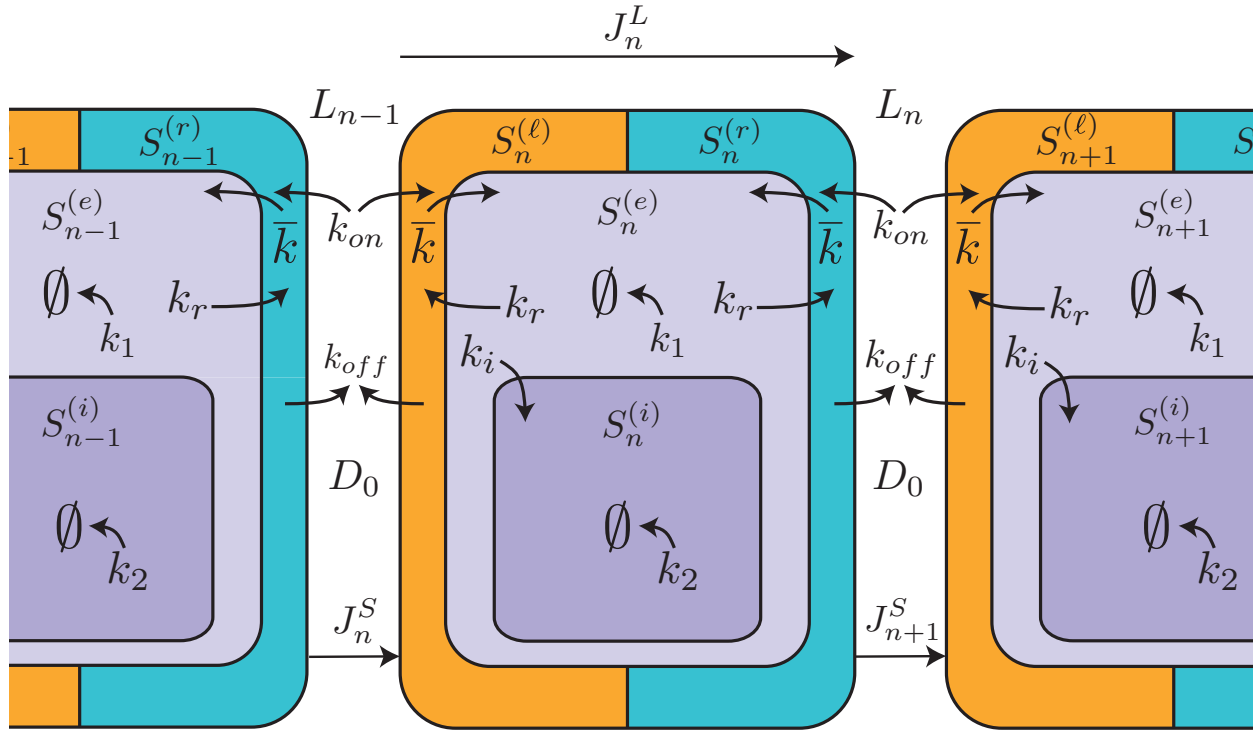


FIG. 6. **Scheme of the morphogen transport model with five cellular compartments**

We introduce pools of receptor bound ligands at the left and right surface of cell n . The molecule numbers in these pools are denoted $S^{(\ell)}$ and $S^{(r)}$, respectively. The number of free extracellular ligand molecules which diffuse with diffusion coefficient D_0 are denoted \bar{L}_n . The molecule numbers in the intracellular mobile and immobile pools are $S^{(e)}$ and $S^{(i)}$, respectively. The binding rate of free ligand to cell surfaces is denoted \bar{k} , k_r is the recycling rate of receptor bound ligands in the mobile pool to the cell surface, molecules of this mobile pool are degraded with degradation rate k_1 , or transfer to the immobile pool with rate k_i . Degradation rate of molecules in the immobile pool is denoted k_2 . The transport fluxes J_n^L and J_n^S are defined in eqs. (B7) and (B8).

2. Dynamic modes of transport

The general solution to the dynamic eqs. (B1) to (B5) can be written as

$$\mathbf{c}_n(t) = \mathbf{c}_n^{ss} + \sum_{\alpha=1}^5 \sum_{m=-N}^N a_m^\alpha \mathbf{c}_m^\alpha e^{iq_m n} e^{-s_\alpha(q_m)t}. \quad (\text{B10})$$

with concentration vector $\mathbf{c}_n = (\bar{L}_n, S_n^{(r)}, S_n^{(l)}, S_n^{(e)}, S^{(i)})$. Here, the time-independent term corresponds to the steady state profile \mathbf{c}_n^{ss} . The time-dependent terms are relaxation modes of wave number q_m and relaxation rate s_α , where $\alpha = 1, \dots, 5$ is a mode index. The mode amplitudes are denoted a_m^α . The boundary conditions are consistent with wave numbers

$$q_m = \frac{2\pi m}{2N+1}. \quad (\text{B11})$$

The relaxation rates and the mode eigenvectors \mathbf{c}_m^α follow from an eigenvalue problem:

$$M(iq_m) \mathbf{c}_m^\alpha = -s_\alpha \mathbf{c}_m^\alpha. \quad (\text{B12})$$

Here $M(z)$ with $z = iq_m$ is the matrix

$$M = \begin{pmatrix} -k_{on} + D_0/a^2 (e^{-z} - 2 + e^z) & k_{off} & k_{off}e^z & 0 & 0 \\ k_{on}/2 & -k_{off} - \bar{k} & 0 & k_r/2 & 0 \\ k_{on}e^{-z}/2 & 0 & -k_{off} - \bar{k} & k_r/2 & 0 \\ 0 & \bar{k} & \bar{k} & -k_r - k_o & 0 \\ 0 & 0 & 0 & k_i & -k_2 \end{pmatrix}, \quad (\text{B13})$$

The eigenvalue problem eq. (B12) defines a characteristic polynomial, $\det[M + \mathbb{I}s] = 0$, where \mathbb{I} is the identity matrix, which reads

$$0 = (k_2 - s) \left[(k_{off} + \bar{k} - s) \left(\bar{k}(k_o - s)(k_{on} - s) - s(k_r + k_o - s)(k_{off} + k_{on} - s) \right) \right. \\ \left. + (\cosh z - 1) \left(\frac{1}{2} \bar{k} k_{off} k_{on} k_r + \frac{2D_0}{a^2} (k_{off} + \bar{k} - s) (\bar{k}(k_o - s) + (k_{off} - s)(k_o + k_r - s)) \right) \right]. \quad (\text{B14})$$

This equation defines a fifth order polynomial equation in s which has five zeros that of wave-length of the eigenmodes of the system. The corresponding eigenvectors \mathbf{c}_m^α follow from eq. (B12). fig. 7 shows an example of the dispersion relations of the five relaxation modes.

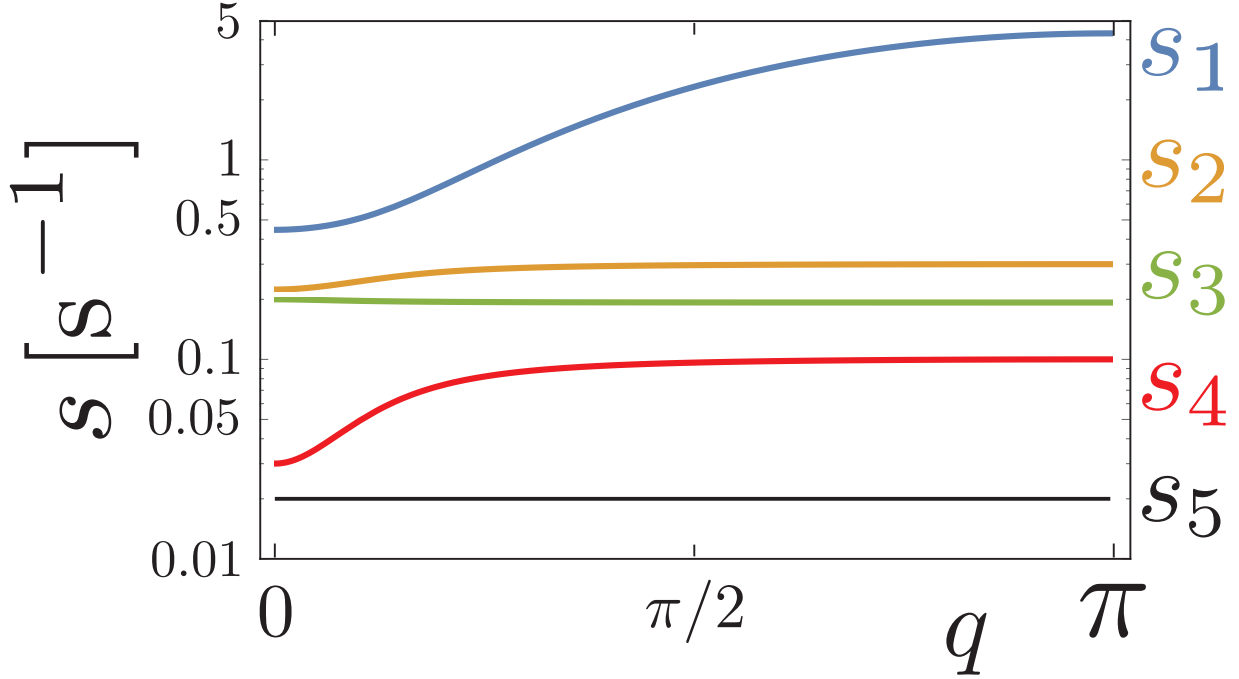


FIG. 7. **Example of the dispersion relations of the five compartment model.** Shown are the relaxation rates s_α as a function of wave number q for the five relaxation modes $\alpha = 1, \dots, 5$ of the full transport model. Parameter values: $D_0 = 10\mu\text{m}^2/\text{s}$, $k_{on} = 0.3/\text{s}$, $k_{off} = 0.1/\text{s}$, $\bar{k} = 0.1/\text{s}$, $k_r = 0.1/\text{s}$, $k_o = 0.1/\text{s}$, $k_2 = 0.02/\text{s}$, $a = 1\mu\text{m}$.

3. Steady-state concentration profiles

Equations (B1) to (B5) can be solved in a piecewise manner for regions of constant production rate. The solution reads

$$\mathbf{c}_n^{ss} = \begin{cases} \mathbf{c}_1^- e^{-\sigma n} + \mathbf{c}_1^+ e^{\sigma n} & -N \leq n \leq -w \\ \mathbf{c}_2^0 + \mathbf{c}_2^- e^{-\sigma n} + \mathbf{c}_2^+ e^{\sigma n} & -w \leq n \leq w \\ \mathbf{c}_3^- e^{-\sigma n} + \mathbf{c}_3^+ e^{\sigma n} & w \leq n \leq N \end{cases} \quad (\text{B15})$$

with concentration vector in steady state $\mathbf{c}_n^{ss} = (L_n S_n^{(r)} S_n^{(\ell)} S_n^{(e)} S^{(i)})$. Amplitudes $\mathbf{c}_i^{(0,-,+)}$ for $i = 1, 2, 3$ are obtained applying boundary conditions as defined above and matching conditions at the boundaries between the three regions. The amplitudes can be written in the form

$$\mathbf{c}_i^{(0,-,+)} = A_i^{(0,-,+)} \mathbf{V} \quad (\text{B16})$$

for $i = 1, 2, 3$, where $\mathbf{V} = [v_1, v_2, v_3, v_4, v_5]$ is a vector with components

$$v_1^0 = 1, \quad (\text{B17})$$

$$v_2^0 = \frac{1}{2} \frac{k_r}{\bar{k} + k_{off}} + \frac{1}{1 + e^{-a\sigma}} \left(\frac{k_o}{\bar{k}} + \frac{k_r}{\bar{k}} \frac{1}{1 + \bar{k}/k_{off}} \right) v_4^0, \quad (\text{B18})$$

$$v_3^0 = \frac{1}{2} \frac{k_r}{\bar{k} + k_{off}} + \frac{e^{-a\sigma}}{1 + e^{-a\sigma}} \left(\frac{k_o}{\bar{k}} + \frac{k_r}{\bar{k}} \frac{1}{1 + \bar{k}/k_{off}} \right) v_4^0, \quad (\text{B19})$$

$$v_4^0 = \frac{1}{2} \frac{k_{on}(1 + e^{-a\sigma})}{k_o + k_{off}/\bar{k}(k_r + k_o)}, \quad (\text{B20})$$

$$v_5^0 = \frac{k_i}{k_2} v_4^0. \quad (\text{B21})$$

The coefficients $A_i^{(0,-,+)}$ are given by

$$A_1^0 = 0 \quad (\text{B22})$$

$$A_1^- = A_2^0 \gamma^{-1} (e^{(2w+1)\sigma} - 1) e^{-(w+1)\sigma} (\chi e^\sigma + \tilde{\chi}) \quad (\text{B23})$$

$$A_1^+ = A_2^0 \gamma^{-1} (e^{(2w+1)\sigma} - 1) e^{(2N-w)\sigma} (-\chi - \tilde{\chi} e^\sigma) \quad (\text{B24})$$

$$A_2^0 = A_2^0 \gamma^{-1} \frac{\nu + 2(A_2^- + A_2^+)(-\xi + \tilde{\chi} + \chi \cosh(\sigma))}{-\xi + \chi + \tilde{\chi}} \quad (\text{B25})$$

$$A_2^- = A_2^0 \gamma^{-1} (\chi \cosh((N-w-1)\sigma) + \tilde{\chi} \cosh((N-w)\sigma)) 2e^{N\sigma} \quad (\text{B26})$$

$$A_2^+ = A_2^0 \gamma^{-1} (\chi \cosh((N-w-1)\sigma) + \tilde{\chi} \cosh((N-w)\sigma)) 2e^{(N+1)\sigma} \quad (\text{B27})$$

$$A_3^0 = 0 \quad (\text{B28})$$

$$A_3^- = A_2^0 \gamma^{-1} (e^{(2w+1)\sigma} - 1) e^{(2N-w-1)\sigma} (-\chi - \tilde{\chi} e^\sigma) \quad (\text{B29})$$

$$A_3^+ = A_2^0 \gamma^{-1} (e^{(2w+1)\sigma} - 1) e^{-w\sigma} (\chi e^\sigma + \tilde{\chi}) \quad (\text{B30})$$

with $\gamma = -2(\chi(\exp(2N\sigma) + \exp(\sigma)) + \tilde{\chi}(1 + \exp((2N+1)\sigma)))$, $\chi = D_0/a^2 + k_r k_{off}/(2(k_{off} + \bar{k}))\Gamma$, $\tilde{\chi} = -D_0/a^2 + k_{off}/(2(k_{off} + \bar{k}))(k_{on} + k_r\Gamma) - k_{on}/2$, $\xi = k_{on}/2$, $\Gamma = k_{on}\bar{k}/(2((k_r + k_i + k_1)(k_{off} + \bar{k}) - k_r\bar{k}))$. The decay rate σ is determined from the condition $\det(M(z = \sigma)) = 0$, which holds for steady states. We then find

$$\cosh \sigma = \frac{1}{2} \left[\frac{k_r}{4k_o} \frac{k_{off}}{(k_{off} + \bar{k})} + \frac{D_0}{a^2 k_{on}} \left(1 + \frac{k_{off}}{\bar{k}} \left(1 + \frac{k_r}{k_o} \right) \right) \right]^{-1} + 1. \quad (\text{B31})$$

with $k_o = k_i + k_1$.

The decay length of the graded distribution of molecules outside of the source is given by

$$\lambda = \frac{a}{\sigma}. \quad (\text{B32})$$

In the limit of large $\lambda \gg a$, the decay length can be approximated as

$$\lambda \approx a \left[\frac{k_r}{4k_o} \frac{k_{off}}{(k_{off} + \bar{k})} + \frac{D_0}{a^2 k_{on}} \left(1 + \frac{k_{off}}{\bar{k}} \left(1 + \frac{k_r}{k_o} \right) \right) \right]^{1/2}. \quad (\text{B33})$$

The decay length λ again has two contributions, one dominated by recycling of molecules at rate k_r and one dominated by extracellular diffusion with diffusion coefficient D_0 . Interestingly, the unbinding rate k_{off} plays an important role for the decay length.

4. Effective diffusion constant and effective degradation rate

We determine effective degradation rates K_α and effective diffusion coefficients D_α by expanding the dispersion relations to second order in wave-length

$$s_\alpha \simeq K_\alpha + D_\alpha q^2 \quad (\text{B34})$$

a. Effective degradation rates

The effective degradation rates are given by $K_\alpha = s_\alpha(q = 0)$. The characteristic polynomial eq. (B14) reads for $q = 0$:

$$0 = (k_2 - s)(k_{off} + \bar{k} - s) \left(\bar{k}(k_o - s)(k_{on} - s) - s(k_r + k_o - s)(k_{off} + k_{on} - s) \right) \quad (\text{B35})$$

which has five zeros. We can identify $s_2 = k_{off} + \bar{k}$ and $s_5 = k_2$. The remaining three zeros can be obtained from

$$\bar{k}(k_o - s)(k_{on} - s) - s(k_r + k_o - s)(k_{off} + k_{on} - s) = 0. \quad (\text{B36})$$

Equation (B36) is a cubic equation

$$s^3 + a_2 s^2 + a_1 s + a_0 = 0, \quad (\text{B37})$$

where

$$a_2 = - (k_r + k_o + \bar{k} + k_{off} + k_{on}) \quad (\text{B38})$$

$$a_1 = (k_r + k_o)(k_{off} + k_{on}) + \bar{k}(k_o + k_{on}) \quad (\text{B39})$$

$$a_0 = - \bar{k} k_o k_{on}. \quad (\text{B40})$$

We define the discriminant of the cubic function as:

$$\Delta = \frac{1}{27} (4\Delta_0^3 - \Delta_1^2), \quad (\text{B41})$$

with

$$\Delta_0 = a_2^2 - 3a_1 \quad (\text{B42})$$

$$\Delta_1 = 2a_2^3 - 9a_2a_1 + 27a_0. \quad (\text{B43})$$

The discriminant is always positive, $\Delta > 0$, which indicates that the cubic function has three real roots. We finally express the effective degradation rates:

$$K_1 = -\frac{1}{3} \left(a_2 - 2\sqrt{\Delta_0} \cos \left(\frac{1}{3} \arccos -\frac{\Delta_1}{2\sqrt{\Delta_0}} \right) \right) \quad (\text{B44})$$

$$K_2 = k_{off} + \bar{k} \quad (\text{B45})$$

$$K_3 = -\frac{1}{3} \left(a_2 - 2\sqrt{\Delta_0} \cos \left(\frac{1}{3} \arccos -\frac{\Delta_1}{2\sqrt{\Delta_0}} - \frac{2\pi}{3} \right) \right) \quad (\text{B46})$$

$$K_4 = -\frac{1}{3} \left(a_2 - 2\sqrt{\Delta_0} \cos \left(\frac{1}{3} \arccos -\frac{\Delta_1}{2\sqrt{\Delta_0}} - \frac{4\pi}{3} \right) \right) \quad (\text{B47})$$

$$K_5 = k_2. \quad (\text{B48})$$

We have chosen the order of rates from fast to slow as in fig. 7.

b. Effective diffusion coefficients

In order to calculate the effective diffusion coefficient for the different modes, we consider the characteristic polynomial for $z = iq$ which has the form

$$(k_2 - s)(s^4 + b_3s^3 + b_2s^2 + b_1s + b_0) = 0. \quad (\text{B49})$$

Here

$$b_3 = -(k_r + k_o + 2(k_{off} + \bar{k}) + k_{on}) - D_0q^2 \quad (\text{B50})$$

$$b_2 = (k_{off} + \bar{k})^2 + (k_r + k_o)(\bar{k} + 2k_{off}) + k_{on}((k_r + k_o) + k_{off} + 2\bar{k}) + \bar{k}k_o + D_0q^2(k_r + k_o + 2(k_{off} + \bar{k})) \quad (\text{B51})$$

$$b_1 = -\left(k_{on}((k_{off} + \bar{k})(\bar{k} + k_o + k_r) + \bar{k}k_o) + (k_{off} + \bar{k})((k_{off} + \bar{k})k_o + k_{off}k_r) \right) - D_0q^2 \left((k_{off} + \bar{k})^2 + 2(k_{off} + \bar{k})(k_o + k_r) - \bar{k}k_o \right) \quad (\text{B52})$$

$$b_0 = (k_{off} + \bar{k})\bar{k}k_0k_{on} + q^2 \left(\frac{\alpha^2}{4} \bar{k}k_rk_{on}k_{off} + D_0(k_{off} + \bar{k})((k_{off} + \bar{k})k_o + k_{off}k_r) \right). \quad (\text{B53})$$

A simple way to solve eq. (B49) this is to rewrite it as a function of its solutions

$$(s - s_1)(s - s_2)(s - s_3)(s - s_4)(s - k_2) = 0, \quad (\text{B54})$$

and expand it in a four degree polynomial to identify coefficients with eqs. (B50) to (B53)

$$b_3 = -s_1 - s_2 - s_3 - s_4 \quad (\text{B55})$$

$$b_2 = s_1(s_2 + s_3) + s_2(s_3 + s_4) + s_4(s_1 + s_3) \quad (\text{B56})$$

$$b_1 = -s_1s_2(s_3 + s_4) - s_3s_4(s_1 + s_2) \quad (\text{B57})$$

$$b_0 = s_1s_2s_3s_4. \quad (\text{B58})$$

From eq. (B49), we observe that the mode with effective degradation $K_5 = k_2$ does not depend on q , thus this is a non-diffusive mode and

$$D_5 = 0. \quad (\text{B59})$$

We then expand eqs. (B55) to (B58) in power series of q up to second order and identify the effective diffusion coefficients as the coefficient of the q^2 -term as a function of the degradation rates K_1, K_2, K_3, K_4 , and the coefficients b_0, b_1, b_2, b_3 defined in eqs. (B50) to (B53), with eq. (17). This process leads to the diffusion coefficients:

$$D_\alpha = \frac{-\sigma_0 + D_0 (K_\alpha^3 - \sigma_1 K_\alpha^2 + \sigma_2 K_\alpha - \sigma_3)}{\prod_{\substack{\beta=1 \\ \beta \neq \alpha}}^4 (K_\alpha - K_\beta)}, \quad (\text{B60})$$

for $\alpha = 1, 2, 3, 4$

with

$$\sigma_0 = \frac{a^2}{4} k_r \bar{k} k_{on} k_{off} \quad (\text{B61})$$

$$\sigma_1 = k_r + k_o + 2(k_{off} + \bar{k}) \quad (\text{B62})$$

$$\sigma_2 = (k_{off} + \bar{k})(\bar{k} + k_{off} + 2k_o) + (2k_{off} + \bar{k})k_r \quad (\text{B63})$$

$$\sigma_3 = (k_{off} + \bar{k})((k_r + k_o)k_{off} + \bar{k}k_o) \quad (\text{B64})$$

Note that $K_i^3 - \sigma_1 K_i^2 + \sigma_2 K_i - \sigma_3 = 0$ for $i = 2$, thus the effective diffusion coefficient of the second mode, does not depend of the free diffusion coefficient, $D_2 \neq D_2(D_0)$, but depends on trafficking parameters.

5. Dispersion relations in the complex plane

To discuss the timescale at which the shape of morphogen gradients is formed during its formation in a five-compartment transport model, we have analyzed the relaxation time spectrum in the complex plane from the zeros of eq. (B14) as $z = \sigma + iq$, see Figure 8. We

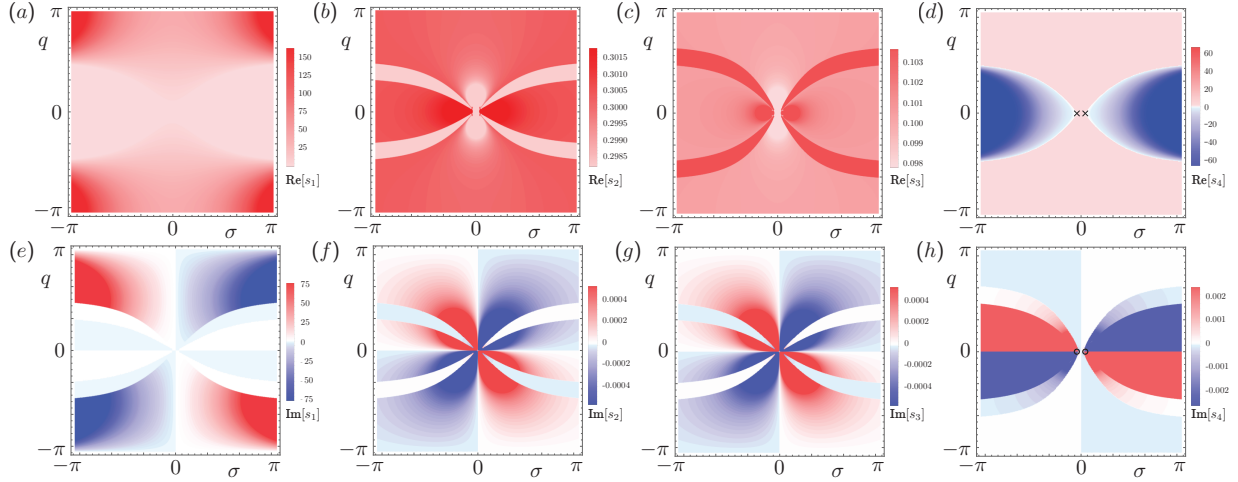


FIG. 8. **Dispersion relation of the five-compartment model in the complex plane.** (a)-(e) Real parts of the relaxation rates s_α with $\alpha = 1, \dots, 4$ as a function of complex wave number $z = \sigma + iq$. (e)-(h) Imaginary parts of the same relaxation rates as in (a)-(e). Values of z for which $s_4 = 0$ are indicated in (d) and (h) by black crosses. Parameter values as in fig. 7

find that only the slow mode s_4 contains points ($q = 0, \sigma = \pm a/\lambda$) in the complex plane with

$$s_4 = 0, \quad (\text{B65})$$

which defines the steady state. Here, the values of σ correspond to the decay length given in eq. (13). Thus, the shape of the distribution of molecules at steady state is determined by the slow diffusive relaxation mode s_4 . And the effective diffusion coefficient and effective degradation rate are D_4 and K_4 , respectively. The expansion of mode $s_4(z)$ for small z gives a similar relation to eq. (17),

$$s_4 \approx K_4 - \frac{D_4}{a^2} z^2. \quad (\text{B66})$$

From fig. 8, the zeros of $s_4(\sigma + iq) = 0$ are given at $q = 0$, then we find that $\sigma^2 \approx a^2 K_4 / D_4$ for $s_4 = 0$, thus we can relate the decay length of the concentration gradient $\lambda = a/\sigma$ with

the effective dynamic parameters of the slow mode s_4 as

$$\lambda \approx \sqrt{\frac{D_4}{K_4}}. \quad (\text{B67})$$

This approximation is valid as long as q and σ are small, which implies that the decay length must be large.

-
- [1] C. H. Waddington, *Organisers and genes* (Cambridge University Press, Cambridge, 1940).
 - [2] A. M. Turing, The Chemical Basis of Morphogenesis, *Philosophical Transactions of the Royal Society of London* **237**, 36 (1952).
 - [3] L. Wolpert, Positional information and the spatial pattern of cellular differentiation., *Journal of Theoretical Biology* **25**, 1 (1969).
 - [4] A. Eldar, D. Rosin, B.-Z. Shilo, and N. Barkai, Self-enhanced ligand degradation underlies robustness of morphogen gradients., *Developmental Cell* **5**, 635 (2003).
 - [5] T. Bollenbach, K. Kruse, P. Pantazis, M. Gonzalez-Gaitan, and F. Julicher, Robust formation of morphogen gradients., *Physical review letters* **94**, 018103 (2005).
 - [6] G. Hornung, B. Berkowitz, and N. Barkai, Morphogen gradient formation in a complex environment: an anomalous diffusion model., *Physical review. E, Statistical, nonlinear, and soft matter physics* **72**, 041916 (2005).
 - [7] K. Kruse, P. Pantazis, T. Bollenbach, F. Jülicher, and M. González-Gaitán, Dpp gradient formation by dynamin-dependent endocytosis: receptor trafficking and the diffusion model., *Development* **131**, 4843 (2004).
 - [8] T. Bollenbach, K. Kruse, P. Pantazis, M. Gonzalez-Gaitan, and F. Julicher, Morphogen transport in epithelia., *Physical review. E, Statistical, nonlinear, and soft matter physics* **75**, 011901 (2007).
 - [9] K. Kruse and A. Iomin, Superdiffusion of morphogens by receptor-mediated transport, *New journal of physics* **10**, 023019 (2008).
 - [10] T. Bollenbach, P. Pantazis, A. Kicheva, C. Bökel, M. González-Gaitán, and F. Jülicher, Precision of the Dpp gradient., *Development* **135**, 1137 (2008).
 - [11] O. Wartlick, P. Mumcu, A. Kicheva, T. Bittig, C. Seum, F. Julicher, and M. Gonzalez-Gaitan, Dynamics of Dpp Signaling and Proliferation Control, *Science* **331**, 1154 (2011).

- [12] P. S. Bosch, R. Ziukaite, C. Alexandre, K. Basler, and Vincent, Jean-Paul, Dpp controls growth and patterning in *Drosophila* wing precursors through distinct modes of action., *eLife* **6**, 375 (2017).
- [13] M. Romanova-Michaelides, D. Aguilar-Hidalgo, F. Jülicher, and M. González-Gaitán, The wing and the eye: a parsimonious theory for scaling and growth control?, *Wiley interdisciplinary reviews. Developmental biology* **4**, 591 (2015).
- [14] D. Aguilar-Hidalgo, S. Werner, O. Wartlick, M. González-Gaitán, B. M. Friedrich, and F. Jülicher, Critical Point in Self-Organized Tissue Growth, *Physical review letters* **120**, 4459 (2018).
- [15] E. V. Entchev, A. Schwabedissen, and M. Gonzalez-Gaitan, Gradient formation of the TGF-beta homolog Dpp., *Cell* **103**, 981 (2000).
- [16] A. A. Teleman and S. M. Cohen, Dpp gradient formation in the *Drosophila* wing imaginal disc., *Cell* **103**, 971 (2000).
- [17] A. Kicheva, P. Pantazis, T. Bollenbach, Y. Kalaidzidis, T. Bittig, F. Jülicher, and M. González-Gaitán, Kinetics of morphogen gradient formation., *Science* **315**, 521 (2007).
- [18] S. Zhou, W.-C. Lo, J. L. Suhalim, M. A. Digman, E. Gratton, Q. Nie, and A. D. Lander, Free extracellular diffusion creates the Dpp morphogen gradient of the *Drosophila* wing disc., *Current biology : CB* **22**, 668 (2012).
- [19] V. P. Chauhan, R. M. Lanning, B. Diop-Frimpong, W. Mok, E. B. Brown, T. P. Padera, Y. Boucher, and R. K. Jain, Multiscale measurements distinguish cellular and interstitial hindrances to diffusion in vivo, *Biophysical Journal* **97**, 330 (2009).
- [20] P. Recho, A. Hallou, and E. Hannezo, Theory of mechanochemical patterning in biphasic biological tissues, *Proceedings of the National Academy of Sciences* **116**, 5344 (2019).
- [21] J. Vollmer, P. Fried, D. Aguilar-Hidalgo, M. Sánchez-Aragón, A. Iannini, F. Casares, and D. Iber, Growth control in the *Drosophila* eye disc by the cytokine Unpaired., *Development* **144**, 837 (2017).
- [22] A. Bläßle, G. Soh, T. Braun, D. Mörsdorf, H. Preiß, B. M. Jordan, and P. Müller, Quantitative diffusion measurements using the open-source software PyFRAP, *Nature Communications* **9**, 1 (2018).
- [23] G. H. Soh and P. Müller, FRAP Analysis of Extracellular Diffusion in Zebrafish Embryos, in *Morphogen Gradients: Methods and Protocols*, *Methods in Molecular Biology*, edited by

- J. Dubrulle (Springer, New York, NY, 2018) pp. 107–124.
- [24] E. G. Magny, J. I. Pueyo, S. A. Bishop, D. Aguilar-Hidalgo, and J. P. Couso, Pegasus, a small extracellular peptide regulating the short-range diffusion of Wingless, *bioRxiv* , 807701 (2019).
- [25] A. B. Kobb, T. Zulueta-Coarasa, and R. Fernandez-Gonzalez, Tension regulates myosin dynamics during *Drosophila* embryonic wound repair, *Journal of Cell Science* **130**, 689 (2017).
- [26] D. M. Umulis, O. Shimmi, M. B. O’Connor, and H. G. Othmer, Organism-Scale Modeling of Early *Drosophila* Patterning via Bone Morphogenetic Proteins, *Developmental Cell* **18**, 260 (2010).
- [27] M. Almuedo-Castillo, A. Bläßle, D. Mörsdorf, L. Marcon, G. H. Soh, K. W. Rogers, A. F. Schier, and P. Müller, Scale-invariant patterning by size-dependent inhibition of Nodal signalling, *Nature Cell Biology* **20**, 1032 (2018).
- [28] A. D. Lander, Q. Nie, and F. Y. M. Wan, Do Morphogen Gradients Arise by Diffusion?, *Developmental Cell* **2**, 785 (2002).